Nanoscale Friction: Measurement and Analysis

Rachel J. Cannara

Center for Nanoscale Science and Technology, National Institute of Standards and Technology

100 Bureau Drive, Mail Stop 6203, Gaithersburg, MD 20899

I. Nanotribology

Tribology is the science and technology of interacting surfaces in relative motion and includes studies of friction, adhesion, lubrication, and wear. Understanding interrelated tribological phenomena is critical for most mechanical devices, as demonstrated by applications in the automotive, aerospace and manufacturing industries. Friction and wear are major causes of mechanical failure and dissipative energy loss. Their impact was first quantified in a study in the United Kingdom which concluded that these losses account for 6 % of the annual gross domestic product in the United States [Jost, 1966; Jost, 1976]. This amounts to greater than $200 billion in 1974 and approximately $800 billion in 2010. In addition, the report predicted that tens of billions of U.S. dollars could be saved by proper use of lubricants. In response to this need, both solid and liquid lubricants have been developed to minimize frictional energy losses, reduce equipment maintenance, and extend device lifetimes. Today, these issues are the focus of significant studies in emerging technologies involving micro- and nanoscale mechanical components and present new technical challenges for tribologists.

The principles of tribology that are relevant to the design of macroscale systems often fail at the nanoscale. This is a result of the ratio of surface to volumetric (or bulk) forces scaling inversely with an object's physical dimensions. Although the mechanical behavior of macroscopic systems is determined mainly by bulk properties and inertia, the ratio between surface and bulk forces increases as length scales decrease. One path towards demonstrating paradigm changes with reduced size is to consider the connection between frictional and gravitational forces. At the macroscale, this is represented by coefficients that relate the normal force (*i.e.*, gravity) on a macroscopic object to friction. At the macroscale, gravitational forces tend to dominate. This is demonstrated by the example described in Figure 1, which compares a 10 cm cube to a 10 µm cube. As the size of the cube is reduced to 10 µm, frictional forces far exceed gravitational forces. As opposed to macroscopic coefficients of friction, the important quantity at smaller scales is the shear strength, τ, which is the *intrinsic* resistance to sliding for a given tribological pair. Expressed in units of (lateral) force per area, at its most fundamental level, τ describes the average force per interfacial atom that must be applied to initiate and maintain sliding between two perfectly smooth surfaces in contact. This paradigm shift in the relation between friction and gravity, where gravity is no longer a relevant normal force, emphasizes the importance of surface effects at reduced length scales, where surface interactions can become devastating for devices.
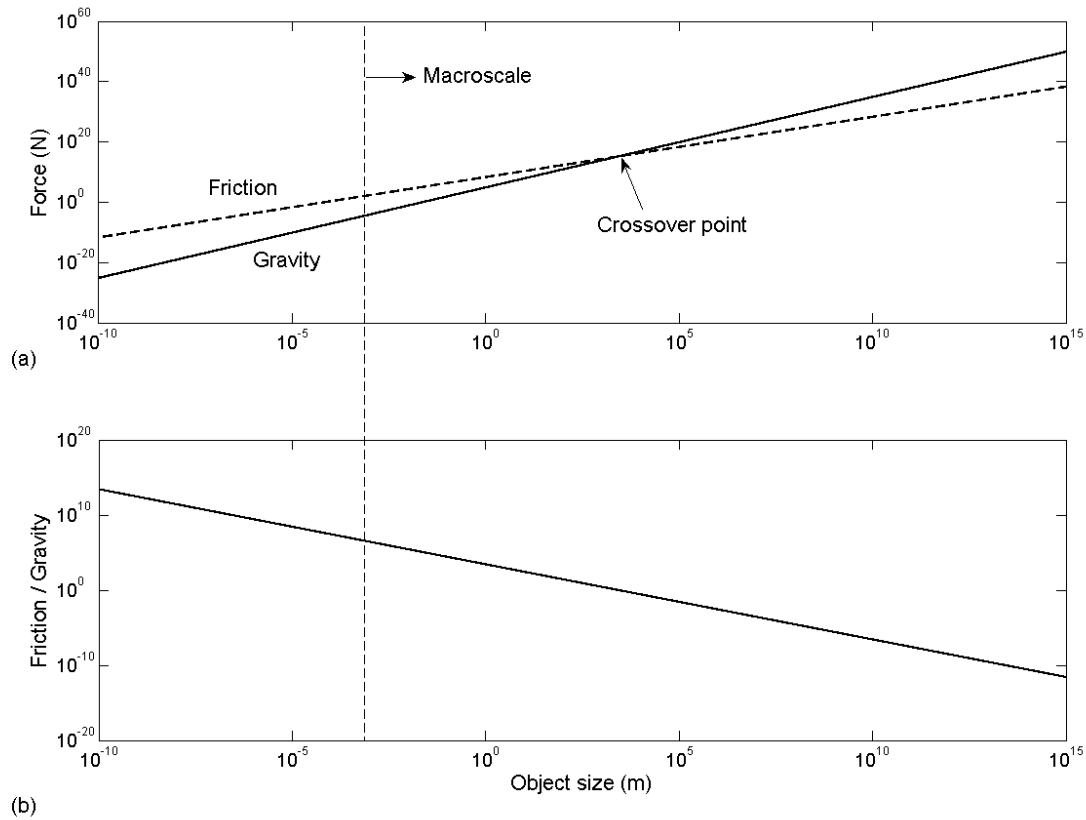
Figure 1. (a) Friction and gravitational forces are plotted as a function of object size, where the object is taken to be a steel cube with a steel-on-steel interfacial shear strength, τ, of 200 MPa and *perfectly smooth* surfaces (*i.e.*, the calculated friction forces arise purely from adhesive load between the two objects and do not account for any surface roughness or additional load due to gravitation). Well into the macroscale, the gravitational force gives an upper limit for friction, assuming a maximum friction coefficient of 1. The crossover point indicates where friction forces begin to dominate gravity as the length scale is decreased. As an example, the force of gravity on a macroscale steel cube with 10 cm-long sides is approximately 100 N. For a 10 μm cube, the gravitational force is reduced by twelve orders of magnitude to 0.1 nN. For perfectly

smooth surfaces, the friction force required to initiate sliding between two identical cubes is equal to τ times the contact area. At 10 cm, this force is 2 MN—an unreasonably high value, because it does not account for any roughness which would reduce the actual contact area (and shift the crossover point to a smaller length scale). At 10 µm, however, the friction force is 20 mN. Despite the unreasonably high *macroscale* friction force calculated in this way and the much lower microscale friction force, the ratio of friction to gravity is still four orders of magnitude greater at the *microscale* than for the macroscale cube. This is illustrated in (b), where the ratio of friction force to gravity is shown to increase as object size decreases. In both (a) and (b), the macroscale regime is assumed to encompass all length scales > 1 mm, as indicated by the dashed vertical line.

Although surface interactions remain important at all scales, lubrication has helped mitigate detrimental surface effects (adhesion, energy dissipation and wear) for many macroscopic systems [Hutchings, 1992; Williams, 1994; Stachowiak, 2005]. A lubricant acts as a buffer between surfaces in sliding contact. It produces interfaces with more favorable chemical or mechanical interactions. As a result, the lubricant-surface or lubricant-lubricant interface screens the unwanted effects of a direct surface-to-surface contact. For macroscopic devices, introducing a lubricant at an interface is generally straightforward. The separations between objects in a micro- or nanoscale system, however, are much smaller and can be less amenable to stable lubrication. In addition, for liquid lubricants, the viscosity of the fluid impedes motion of micro- and nanoscale parts, and its surface tension can cause these parts to warp and adhere. Hence, while macroscale lubrication schemes often rely on the formation of a solid or liquid interface

where a lubricant slides against itself, tribological principles applicable to micro- and nanoscale devices (*i.e*., nanotribology) must focus primarily on surface interactions at the original interface. This fundamental difference is key to understanding and controlling friction at the nanoscale.

Tribological phenomena have slowed the development of micro- and nanomechanical systems (M/NEMS), limiting their commercial application to those systems that do not include contacting sliding interfaces [Romig, 2003]. MEMS components tend to stick together as a result of large surface forces. This "stiction" behavior poses an engineering problem both for the device itself and its process design. For example, the drying step in a liquid etch or release process forms menisci whose surface tension forces freestanding mechanical parts into irreversible contact. Researchers have improved this process by using freeze-drying, supercritical CO_2 drying, or laser heating to prevent or reverse stiction due to capillary meniscus formation [Guckel, 1990; Mulhern, 1993; Fushinobu, 1996; Phinney, 2000; Rogers, 2002]. More examples can be found elsewhere in comprehensive reviews of the tribological properties of MEMS [Maboudian, 1997; Romig, 2003; Maboudian, 2003; Williams, 2006; Kim, 2007]. Despite many important advances, failure is unavoidable for most MEMS devices (*e.g.*, gears, locks, shutters, optical switches, *etc*.) that incorporate *sliding* interfaces.

The best performance to date was demonstrated by a silicon MEMS tribometer [Asay, 2008a & 2008b], a MEMS device designed for measuring micro- and nanoscale tribological properties. With a lifetime of at least 11 days, corresponding to 10^8 cycles, the contact traversed more than 1.5 kilometers. At that point, the test was halted, but failure was not yet observed. This extended lifetime is a result of a self-replenishing, vapor-phase lubricant and represents a vast improvement over previous results. At least tens of billions of cycles and demonstration of

uniform endurance across many devices operating in parallel would be required for a device to be commercially viable. In a promising advancement for MEMS reliability, Texas Instruments was successful in producing light projectors consisting of an array of digital micromirror devices (DMDs) that function by switching between two orientation angles, corresponding to "on" and "off" positions. DMDs rely on both an advanced (vapor-phase) lubrication scheme [Henck, 1997] and the constant mechanical oscillation of the mirror yolk to prevent adhesion of the yolk's contact points to the landing pads. DMDs have been commercialized successfully, but their functionality does not rely on a sliding interface. Further advanced systems that incorporate many sliding interfaces will require lubrication schemes with a level of sophistication on par with the complexity of the device.

As these processing and operational barriers are overcome, and premature failure due to adhesion and wear are eliminated, issues of energy dissipation that continue to pose challenges for electronic devices will become equally important for M/NEMS. Frictional energy dissipation can be very low for individual nanoscale contacts, which consist of only tens or hundreds of atoms. But complex M/NEMS devices involve many of these single-asperity contacts operating in parallel [Romig, 2003]. Using conservative values for the friction force for a single-asperity (1 nN to 100 nN) and for the sliding velocity (10^{-6} m/s to 10^{-2} m/s), the frictional energy dissipated by a single nanoscale contact can range from a femtowatt (1 fW = 10^{-15} W) to a few nanowatts (1 nW = 10^{-9} W). However, at more technologically relevant sliding velocities (*i.e.*, > 1 mm/s), these losses are more than the total effective power dissipated by a single silicon transistor in an integrated complementary metal-oxide-semiconductor (CMOS) circuit. (At maximum allowed power densities, a modern transistor dissipates approximately one-tenth of a

picowatt (1 pW = 10^{-12} W) [Lin, 2008].) Furthermore, nanoscale asperities are more densely packed than CMOS transistors, possibly increasing the total energy dissipated per area and ultimately lost as heat. M/NEMS employing components that rely on sliding contacts comprise thousands of nanoscale contacts per device. Assuming over a million devices operating in parallel (as in a micromirror array), with each device consisting of thousands of single-asperity contacts sliding at more than 1 mm/s, up to several Watts of input power will be lost to friction alone. Hence, the ability to tune friction either by surface treatments or tailored substrate materials is critical for the future of complex M/NEMS technologies.

Toward this end, this chapter describes the tools and models used to understand the fundamental properties of friction at the nanoscale. Section II provides a description of the atomic force microscope (AFM) and explains how the AFM is used to measure friction and extract shear strength, work of adhesion, and other important properties. The goal is to provide a starting point for researchers interested in performing nanoscale friction measurements, using the most widely available instrumentation and contact models. Section III concludes with a brief discussion of new measurement techniques and modeling challenges important for the development of commercially-viable devices.

II. Friction force microscopy

The first measurement of nanoscale friction was performed by Mate, McClelland, Erlandsson and Chiang in 1987 [Mate, 1987]. They observed atomic-level stick-slip behavior on graphite: The atoms on the nanoscale apex of a tungsten AFM tip would stick and slip laterally along the

surface with the spatial periodicity of the graphite(0001) lattice below. An example of the same type of stick-slip behavior is shown in Figure 2 for an AFM tip sliding on freshly-cleaved sodium chloride. Binnig, Quate and Gerber had invented the AFM over a year prior to Mate's remarkable discovery [Binnig, 1986]. They modified the scanning tunneling microscope (STM) [Binnig, 1982; Binnig, 1983] by affixing a diamond probe to a small, compliant cantilever placed between an STM tip and the sample surface. This configuration permitted them to measure and to vary the forces between the probe tip and sample surface with sub-nanoNewton precision. Here, the tunneling current between the STM tip and the conductive Si cantilever was used to measure the displacement of the free end of the compliant cantilever and therefore the normal load applied to the sample. The spatial resolution of the instrument approached atomic-scale precision. The AFM thus enabled both force and topographical measurements on *insulating* and conducting surfaces, alike, with high resolution. In their pioneering nanoscale friction experiments, in which they also observed atomic-level stick-slip for the first time, Mate *et al*. used optical interferometry (instead of an STM approach) to sense the *torsion* of the cantilever and thereby measure *lateral* forces at the atomic-level.

Later, the use of a laser beam position-sensitive detector (PSD) became the primary approach for sensing the minute angular deflections of the cantilever beam [Meyer, 1988; Meyer, 1990a; Alexander, 1989]. As in the original STM-based AFM, the cantilever would bend in response to nanoscale forces on the probe tip attached at its free end. In the approach using a PSD, however, the change in angle of the cantilever translates to a change in angle of reflection of a laser beam incident on the reflective backside of the cantilever. The position of the laser spot on the photodetector depends on this reflection angle, and the resulting "deflection" signal can be

calibrated in units of force (as described below) and used to determine the applied load in an experiment. Most measurements of nanoscale friction extend this optical-beam-deflection technique to measure the torsion of a cantilever beam in response to lateral forces. In fact, the two groups of Marti, Colchero and Mlynek [Marti, 1990] and of Meyer and Amer [Meyer, 1990b] expanded upon this method to record the normal and lateral displacements of the laser beam *simultaneously*. (The normal and lateral signals correspond to the bending and torsional response of the cantilever, respectively.) The ability to record these two signals separately but simultaneously enables coincident bending and torsion measurements, such as the one shown for graphite in Figure 3. Today, this dual-force optical-beam-deflection method is the most common technique used in friction force microscopy (FFM). Many important FFM studies have relied on the instrumentation described above, and extensive reviews which together map out the history of measurement and experiments in nanotribology can be found elsewhere [Carpick, 1997a; Hähner, 1998; Meyer, 1998; Persson, 2000; Gnecco, 2001; Krim, 2002; Colton, 2004; Szlufarska, 2008].
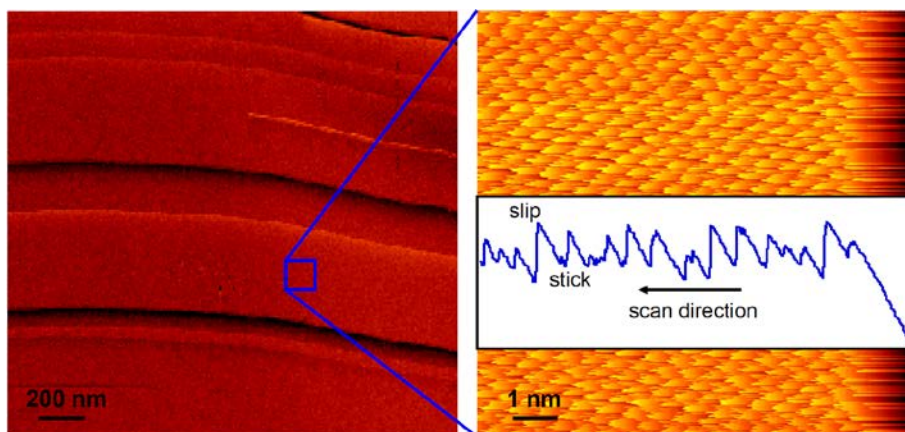
Figure 2. Left: 2 µm x 2 µm AFM deflection image of atomic terraces on the (001) face of a freshly-cleaved sodium chloride crystal in ultrahigh vacuum. (The curvature is caused by drift in the piezoelectric scanner.) Right: A 10 nm x 10 nm stick-slip image and cross-section resolving the atomic lattice on the terrace indicated to the left. (The lattice constant of NaCl is 0.564 nm.)
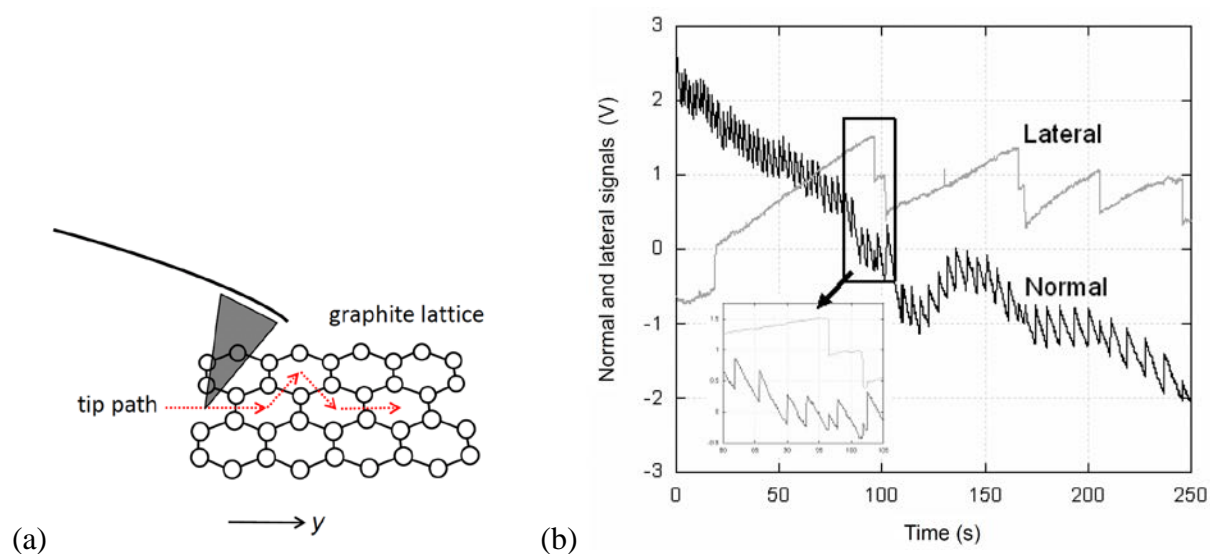

(a)   (b)

Figure 3. (a) Schematic representation of an AFM tip sliding along the graphite(0001) lattice, indicating a possible tip path, which can deviate from the direction (y in this depiction) along which the sample or tip base is scanned. (b) Stick-slip occurring as a function of time while the sample is moved vertically. The cantilever bends and releases, because its tilt angle (in this case, 22.5°) with respect to the sample couples z-motion into a tip-sample displacement along y. This forces the tip (silicon nitride, with $k_N = (0.022 \pm 0.001)$ N/m) to slide along the freshly-cleaved graphite surface, resulting in stick-slip behavior. Most of the stick-slip events occur along y; however, jumps along x are also observed. This occurs when the tip slips sideways into a nearby

honeycomb structure, as indicated in (a). The inset in (b) reveals the half-jumps in the normal signal that coincide with each of these lateral slip events.

The AFM controls the position of the fixed end of the cantilever which permits indirect control over the applied load in an experiment, with the load range and sensitivity depending on the spring constant of the cantilever. As a result, the AFM is prone to snap-in and pull-off (snap-out) instabilities, which occur at a tip-sample separation where the interaction force gradient matches the cantilever spring constant. Another highly valuable but less common scanning probe instrument used to investigate tribological properties is the interfacial force microscope (IFM) [Joyce, 1991]. Through the use of a capacitive platform to sense cantilever deflection, the IFM enables direct control over the applied load and is therefore immune to the instabilities inherent to the AFM. The original purpose of the IFM was to investigate mechanical properties and adhesion by controlling tip-sample separation [Houston, 1992]; it was not explicitly designed for performing FFM measurements. Nonetheless, it has been used in several cases for friction measurements in the tensile regime, where AFM measurements can be challenging [Burns, 1999; Kiely, 1999; Kim, 2000a; Houston, 2002; Major, 2003; Major, 2006]. However, quantitative analysis of friction measurements in an IFM is limited, because it is difficult to separate the torsional signal (due to friction) from the normal force signal and to calibrate each force independently.

The ability to measure normal and lateral signals simultaneously is essential for measuring nanoscale friction, as the properties of friction, including stick-slip behavior and the magnitude of friction forces, are typically load-dependent. The linear load-dependence observed at the

macroscale arises from the micro- and nanoscale roughness of the contacting surfaces causing an increase in true contact area with increasing load: As the pressure on each protrusion (or "asperity") increases, the contacting asperities deform and flatten [Greenwood, 1966], and this elastic (and sometimes plastic) deformation reduces the overall gap between the surfaces and permits shorter protrusions to make contact with the counter-surface, increasing total contact area. Accordingly, the familiar (macroscale) coefficient of friction, which is taken to be equal to the slope of the friction-load curve, is not an intrinsic property of an interface, because it depends on surface geometry (*e.g*., roughness) and wear. Therefore, it is important to measure friction for individual nanoscale asperities in order to extract truly intrinsic quantities. While friction is load-dependent even at the single-asperity level, the advantage of performing friction measurements at the nanoscale is the relative ease with which the contact geometry may be modeled and the ability to identify and avoid atomic-level wear by precise control of contact pressures.

In this regard, continuum mechanics has proved to be a useful tool for determining the load dependence of the tip-sample contact area. Contrary to macroscopic observations, Bowden and Tabor found that friction is proportional to the true area of contact [Bowden, 1985]. Consequently, if the area-load relation is known, a friction-load plot can reveal critical information about the interface, including the work of adhesion, pressure dependence and wear properties. Continuum mechanics models can yield quantitative area-load relationships when the elastic properties of the two contacting materials are known. It should be noted, however, that the breakdown of continuum mechanics at the nanoscale is a critical topic of ongoing interest, and caution must be used when applying a continuum fit to nanoscale friction-load data [Luan, 2005 & 2006; Mo, 2009]. This breakdown can occur when atoms are treated as discreet entities, as

opposed to forming a smooth, continuous line of material that fills and defines the boundaries of an object. Measuring nanoscale contacts and forces with sub-nanoNewton precision gives us insight into potentially the most fundamental mechanisms of friction at all scales, but it also means that these data are more sensitive to microscopic laws. Fortunately, while the most appropriate analysis approach is not yet established nor fully understood for each experimental system, free parameters that emerge from continuum methods can be checked for consistency with separately calculated physical quantities, as discussed in detail below.

Before describing the continuum mechanics models, it is important to discuss the apparatus and data collection procedure. Simultaneous measurement of normal and lateral signals in an AFM requires a four-quadrant PSD (instead of only two photodiodes required for a simple normal force measurement). Rastering of the probe tip over the sample is accomplished by actuating a piezoelectric (piezo) scanner in the xy plane, while controlling z-motion to maintain constant height or applied load. Figure 4 shows a basic schematic of an AFM, including the (now-standard) four-quadrant detector, xyz scanner with sample, and a rectangular cantilever and probe tip. The scanner designs vary depending on the instrument, with major differences being the decoupling of the z-piezo from the xy stage and the use of closed-loop scanners to ensure accurate displacements.
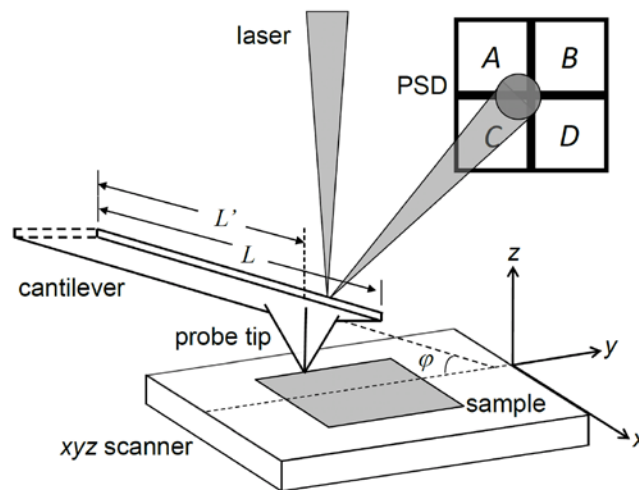
Figure 4. Schematic of an AFM employing the typical optical-beam-deflection technique. Components include a cantilever and probe, four-quadrant PSD, *xyz* scanner, and sample. Both the full length, *L*, of the cantilever and distance between the tip and cantilever's base, *L'*, are indicated. The angle, *φ*, corresponds to the incline of the cantilever's long axis with respect to the *xy* plane of the scanner.

The deflection, or "normal," signal, V_N, is obtained by subtracting the top (A and B) and bottom (C and D) PSD quadrants indicated in Fig. 4:

$$V_N = (V_A + V_B) - (V_C + V_D). \tag{1}$$

Likewise, the difference between left and right quadrants gives the lateral signal, V_L:

$$V_L = (V_A + V_C) - (V_B + V_D). \tag{2}$$

Both the normal and lateral signals scale with the total, or "sum," signal of all the quadrants. Dividing out the sum signal is sometimes performed but unnecessary, as long as the normal and lateral force calibration factors account for any changes in total signal. In a nanoscale friction measurement, the applied load is typically ramped line-by-line in the AFM image, as the tip rasters over the sample in the xy plane. By scanning forward and backward in the $+x$ ("trace") and $–x$ ("retrace") directions, respectively, a friction loop is recorded at each applied load. Figure 5a shows a basic friction loop. To remove contributions from the lateral signal offset, the friction force is obtained by calculating the half-width of the loop (as in Fig. 5a), equal to half of the difference between the trace and retrace signals. Friction is then calibrated in units of force, using methods described below. The load is varied either by adjusting the z-piezo position or by directly controlling the deflection set-point in a feedback loop with the z-piezo. In either case, each load will be applied to different locations on the sample, as significant displacement of the tip along the y-direction occurs due to the tilt of the cantilever. This effect (exemplified in Fig. 3b) was first observed by Watson *et al*. [Watson, 2004] and can be countered with a scanner displacement in the direction opposite to the lateral tip displacement, as described elsewhere [Cannara, 2005].

As shown for the stick-slip measurement on muscovite mica in Fig. 5b, x-scan sizes as low as a few nanometers may be used, depending on the length of the initial sticking portion of the friction loop (*e.g*., line ab in Fig. 5a and between 0 nm and 0.75 nm in the upper trace of Fig. 5b). The applied load typically ranges from a maximum of one to three times the adhesive force to a minimum value at pull-off (where the applied load is equal and opposite to the adhesive force). The value of the maximum applied load is selected to avoid wear of the tip or sample surface or

to obtain sufficient data for a continuum fit. The resulting data consist of a set of three

simultaneously-recorded images: (1) the raw deflection (normal) signal, (2) the lateral signal in

the trace direction, and (3) the lateral signal in the retrace direction. The normal signal image

contains an out-of-contact portion, which indicates the normal signal offset. This offset is

subtracted from a line-by-line average of the image, which can then be calibrated in nN, as

described in the next paragraph. The friction force is calculated from the difference between

images (2) and (3) to obtain the half-width, as discussed above. To remove contributions from

the sticking portion (line ab in Fig. 5a) of the data, only the region between the two vertical

dashed-dotted lines in Fig. 5a is included in the analysis.
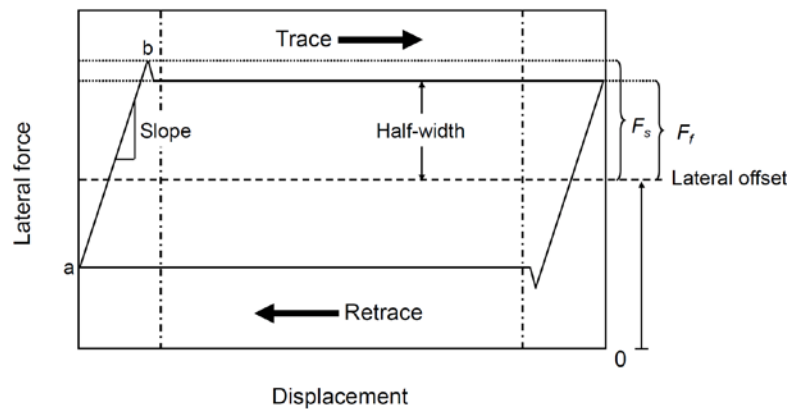
(a)
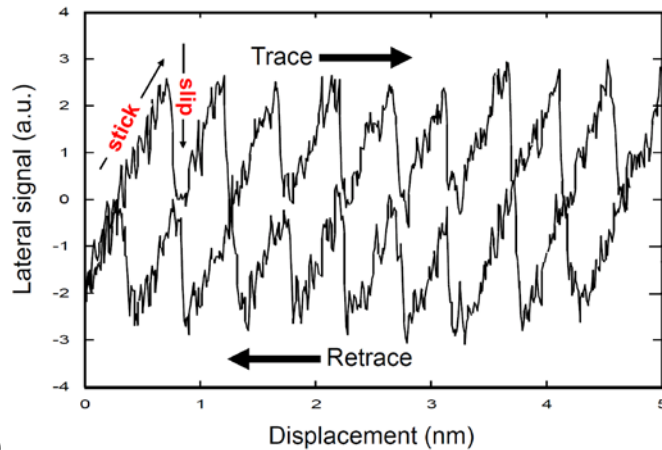
(b)

Figure 5. (a) Schematic friction loop consisting of a lateral offset (due to optical crosstalk and/or the geometry of the surface) and lateral forces measured in both the trace and retrace directions. A trace (or retrace) scan begins with the sticking portion indicated by line ab, whose slope corresponds to the total lateral stiffness of the cantilever-tip-contact system. Once the tip overcomes the lateral sticking force, F_S, it slides at the dynamic friction force, F_L, which can be determined from the half-width of the friction loop bounded by the two vertical dashed-dotted lines. (b) Stick-slip friction on freshly-cleaved muscovite mica in ambient air. The stick and slip events repeat with the spatial periodicity of the mica lattice (≈ 0.529 nm). The top and bottom traces correspond to scanning the tip along forward (to the right) and reverse (to the left) directions, respectively.

The normal force, F_N, is calibrated with the normal spring constant of the cantilever and the deflection sensitivity of the optical system. While nominal values for the normal spring constant, k_N, are often supplied by the manufacturer, these values can differ significantly from their actual

values. Sader and co-authors have developed rapid, quantitative methods for determining the spring constants of cantilevers of various shapes (*e.g.*, rectangular, triangular, *etc.*), using the plan view dimensions of a cantilever and its resonance properties in air [Sader, 1999; Green, 2004; Sader, 2005]. Both the resonance frequency and quality factor may be determined by oscillating the cantilever in the AFM and measuring the response at different frequencies. This measurement must be performed in air (or in a medium with a sufficient viscosity) to accommodate the use of a hydrodynamic damping function in the calculation of k_N. Other reliable methods obtain resonance properties and spring constants based on the shift in fundamental-mode frequency due to an added mass [Cleveland, 1993; Green, 2004] or from the thermally-induced oscillations (or "thermal noise") of the cantilever [Hutter, 1993; Butt, 1995; Burnham, 2003]. Alternatively, the spring constant of individual cantilevers can be determined directly by pressing against a reference cantilever of precisely known stiffness [Gibson, 1996; Tortonese, 1997; Gates, 2007].

The spring constant of the *full* length of the cantilever is given by k_N, but the relevant spring is a function of the location along the cantilever's long axis where the load is actually applied in the experiment. Hence, if a calibration method determines k_N, it is necessary to measure the location of the tip and calculate an effective spring constant, k_N', according to the following equation:

$$k_N' = k_N \left(\frac{L}{L'} \right)^3 , \tag{3}$$

where L is the full length of the cantilever, and L' is the distance from the base of the cantilever to the tip location along the cantilever's long axis. The deflection sensitivity, S_N, is the measured change in normal signal per change in z-displacement, when the tip is pressed against a *rigid* sample, such as silicon. (To measure S_N accurately, no sample or tip deformation may occur.) The normal force calibration factor, C_N, is then given by:

$$C_N = \frac{k'_N}{S_N \cos^2 \varphi}. \tag{4}$$

The cosine-squared term accounts for the tilt angle, φ, of the cantilever with respect to the sample plane (Fig. 4) to obtain the component of the force that is normal to the surface and the projection of the z-displacement perpendicular to the cantilever in the yz plane. Further consideration of the impact of cantilever tilt on force calibration yields a more complicated relationship, depending on the tip location, geometry and tip-sample interaction, as studied elsewhere [Stiernstedt, 2005; Edwards, 2008]. Once the calibration factor is known for a specific experiment, accounting for tip location and cantilever tilt, the applied and total (applied plus adhesive) loads in the experiment can be calculated by multiplying the deflection signal (minus its offset) by C_N.

Calculating the lateral force calibration factor, C_L, is more complicated than the normal force calibration procedure. However, several approaches have been developed that are relatively straightforward [Munz, 2010]. Each method falls along a spectrum that varies from the direct experimental determination of C_L to analytical or numerical methods, and the appropriate technique for a given experiment is chosen based on its accuracy, ease of use, and whether it is acceptable to risk damage to the tip. The most widely applicable techniques may be grouped

under two headings defined here as "relative" and "direct." Relative methods require prior knowledge of either k_N or C_N to determine C_L, and direct methods do not. For example, the "wedge" method [Ogletree, 1996; Varenberg, 2003; Tocha, 2006], originally developed by Ogletree *et al.*, is an indirect method, as its output is the ratio between lateral and normal force calibration factors, and a linear friction-load relationship is assumed in the derivation of this ratio. The wedge method is a well-established lateral force calibration technique and a standard to which newer methods are often compared. But it should be noted that the technique, itself, is a friction-load experiment performed on a two-sloped calibration sample (*e.g.*, 1 µm to 2 µm-high (111) silicon facets) and thus incurs some risk of contamination and permanent damage to the tip. Performing the calibration with a separate, identical probe is possible but adds error to the measurement.

There are at least three calibration procedures that do not require sliding the tip over the surface of a calibration sample, where both are *direct* calibration methods. The "test probe" method [Cannara, 2006; Chung, 2010] is the lateral analogue to the normal force calibration procedure. It is therefore a direct method but requires knowledge of the cantilever's torsional spring constant, k_L, which can be obtained via the torsional Sader method [Green, 2004] and an understanding of the in-plane deformation of the cantilever [Sader, 2004]. In the test probe method, a spherical probe is attached to the free end of the cantilever, and a lateral force-displacement curve is obtained by pushing the probe against a rigid, vertical wall. The lateral deflection sensitivity (calculated from the force curve), along with k_L and the size of the sphere, yield the lateral force calibration factor, C_L. Depending on the experiment, C_L may then be used to calculate the calibration factor for a cantilever-*tip* combination with a similar cantilever

geometry or for the same cantilever with a sphere glued to the end post experiment. This is valid, as long as the lateral stiffness of the tip shaft is large compared with the torsional spring constant. Alternatively, if the sphere itself is used both for calibration and experiment (instead of a tip), the respective contact points are the side and apex of the sphere, respectively, and tip stiffness can be neglected due to the low aspect ratio of the spherical probe. All variations of the test probe method avoid contacting the probe apex to a calibration sample, which is advantageous for probes with sensitive or unique end structures or coatings. If there is contamination or wear, it is then certain that it occurred during the experiment and not during the calibration procedure.

Direct calibration of lateral forces without prior knowledge of k_L is achieved using the diamagnetic lateral force calibrator (D-LFC), which consists of a static friction measurement on a pyrolitic graphite sample levitating over four permanent magnets [Li, 2006]. The tip makes contact with the sample, but no sliding occurs when the procedure is performed properly. Moreover, the freshly-cleaved graphite surface is clean and inert, minimizing the possibility of tip damage. Unlike the test probe method, k_L is not required. Although the cantilever's spring constants remain unknown, the spring constant of the levitation system is characterized by a ring-down measurement, which yields the frequency and quality factor for the levitating sample as it oscillates about the minimum of the magnetic field. The main premise of the D-LFC method is that the levitation spring constant is so much lower than the contact spring and the torsional spring constant of the cantilever that the lateral displacement of the tip is negligible in comparison with the lateral displacement of the sample. As a result, the static friction data represent the torsional response of the cantilever to a force approximately equal to the scan size times the levitation spring constant. Much like the test probe and normal force calibration

equations, the slope of the lateral signal as a function of scanner displacement (typically in V/nm) can be divided by the levitation spring constant to obtain C_L. This direct calibration of C_L provides a clever way of avoiding the limitations suffered by other static methods [Cain, 2001].

A third direct lateral force calibration technique determines C_L by exerting a torque at a known distance from the long axis of the cantilever near the tip location [Feiler, 2000]. Reitsma *et al*. improved upon this "pivot" method by performing the measurement at multiple pivot points. Their approach requires either a special "hammerhead" probe [Reitsma, 2007] or a wide enough cantilever beam such that multiple distinct locations near the free end of the cantilever may be loaded [Chung, 2007]. The result is a simultaneous measurement of the torsional spring constant of the cantilever beam and the lateral deflection sensitivity of the optical system. The benefits of this calibration technique include the lack of sliding or contacting the tip to a calibration surface and the absence of any lateral scanning which would require a calculation of in-plane bending [Sader, 2004]. As with all methods, the effect of cantilever tilt on force calibration remains important, as tilt can have a significant impact on both normal and lateral force calibration factors, alike [Stiernstedt, 2005; Edwards, 2008]. The pivot method may also be used to determine k_L.

A note about probe materials: Probe tips may consist of a variety of conducting or insulating materials. While silicon or silicon nitride can be etched from a single crystal, variations in tip materials are typically achieved by coating silicon probes (*e.g*., with titanium nitride, silicon nitride, tungsten carbide, platinum, *etc*.) Much effort, however, has gone into producing monolithic structures composed of hard materials, including diamond, polycrystalline diamond and diamond-like carbon (DLC) [Sullivan, 2001; Sekaric, 2002; Olivero, 2006; Peiner, 2007;

Luo, 2007]. Similar to the silicon or silicon nitride cantilevers, in a monolithic structure the entire cantilever-probe combination is made of one continuous structural material. *Unlike* silicon or silicon nitride, amorphous or polycrystalline diamond is deposited instead of etched. To date, no monolithic single-crystal diamond cantilever-probe combination has been reported; however, Obraztsov *et al*. recently developed a technique for producing individual diamond tips on silicon cantilevers by a series of chemical vapor deposition, oxidation and silicon etch steps [Obraztsov, 2010]. To obtain *amorphous* diamond tips, Bhaskaran *et al*. deposited DLC into molds in silicon and fabricated silicon cantilevers with DLC tips [Bhaskaran, 2010]. It is also possible to coat tips with DLC and various hydrocarbon materials by electron beam-induced deposition (EBID) in an electron microscope [Schwarz, 1997]. The scanning electron microscope and the transmission electron microscope (TEM) are useful for both EBID and tip-shape measurements [Derose, 1997; Kopycinska-Müller, 2006]. In particular, the TEM is indispensable for high-precision measurements of tip geometry (*e.g*., radius of curvature), coating thickness, and local atomic structure. As will be evident in the data analysis discussion to follow, an accurate tip radius measurement is critical for extracting quantitative information from friction-load curves.

At least two important quantities are obtained from nanoscale friction measurements: the shear strength (τ) and the work of adhesion (*w*). As described above, τ is the intrinsic resistance to sliding. The work of adhesion is the energy per unit area that must be supplied to pull two surfaces apart. It can be quantified in terms of surface energies:

$$w = \gamma_1 + \gamma_2 - \gamma_{12}, \tag{5}$$

where γ_1 and γ_2 correspond to the energies of formation of the two surfaces, and γ_{12} corresponds to the energy required to create the interface. For identical surfaces, γ_{12} is equal to zero; for dissimilar materials, elastic deformation or the off-equilibrium positioning of interfacial atoms leads to additional (potential) energy stored in the contact, which is then regained upon separation. In general, w will affect the magnitude and load dependence of the tip-sample contact area and, consequently, the friction force. However, to first order, τ is independent of w.

The shear strength can depend upon parameters such as pressure, temperature and velocity [Briscoe, 1982], to name a few. As mentioned above, the friction force, F_L, is proportional to the contact area, A, with τ the constant of proportionality [Bowden, 1985]:

$$F_L = \tau A .\qquad(6)$$

The dependence of τ on pressure, P, is often assumed to be linear:

$$\tau = \tau_0 + \zeta P .\qquad(7)$$

To first order, however, it can be assumed that the shear strength has no pressure dependence ($\zeta = 0$), and the shape of the friction-load curve is determined solely by the change in A with applied load. Figure 6 provides an example of a friction-load curve for a hydrocarbon-coated tip sliding on microcrystalline diamond in dry nitrogen (150 nm tip radius, 20 nm scan size). The solid line is a curve fit assuming a constant shear strength and using the continuum methods described below.
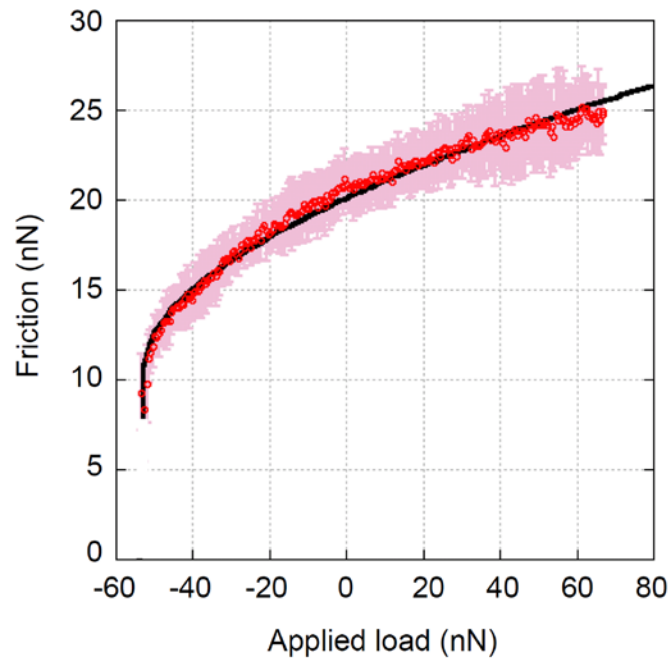
Figure 6. Friction plotted as a function of applied normal load (open circles); error bars are the standard deviations from the mean indicating the curve-to-curve variation. The data are fit by the COS transition model (solid black line), representing the dependence of contact area on applied load.

The area-load relationship is a function of tip radius, *R*, the elastic properties of the two materials, and the magnitude and range of their interaction (*i.e.*, *w*). These physical properties determine the location of the interface along a continuous theoretical spectrum bounded by two continuum mechanical extremes [Greenwood, 1997]. Specifically, the physical properties of the interface determine the fraction of elastic deformation that occurs due to adhesion of the unloaded interface with respect to the overall range of interaction between the two surfaces. This ratio is called Tabor's parameter and is given by [Tabor, 1977]:

$$\mu_T = \left(\frac{16Rw^2}{9K^2 z_0^3} \right)^{1/3},$$

(8)

where z_0 is the equilibrium separation for a Lennard-Jones interaction potential, and

$K = \frac{4}{3} \left(\frac{1-v_{tip}^2}{E_{tip}} + \frac{1-v_{sample}^2}{E_{sample}} \right)^{-1}$ is the combined (or "reduced") elastic modulus, given by the

Poisson's ratios, v, and Young's moduli, E, of the tip and sample. At one end of the spectrum,

the contact deformation is significant compared with the range of interaction (z_0), and μ_T is also

large. In this case, the area-load relationship is described by Johnson-Kendall-Roberts (JKR)

theory [Johnson, 1971]. At the other end of the spectrum, the deformation is small compared

with z_0. Thus, μ_T is small, and the contact follows Derjaguin-Muller-Toporov (DMT) theory

[Derjaguin, 1975]. Intermediate regimes exist between these two extremes, and the

corresponding transition from JKR to DMT has been described analytically by Carpick, Ogletree

and Salmeron (COS) [Carpick, 1997b] and given its physical basis by Schwarz [Schwarz, 2003].

The generalized transition, or "COS," equations have made the JKR-DMT analysis easily

applicable to nanoscale friction measurements [Grierson, 2005].

In general, the following COS equation describes the dependence of the contact area on

normal load, F_N, for a sphere(or paraboloid)-on-flat geometry:

$$A = A_0 \left(\frac{\alpha + \sqrt{1 - F_N/F_C}}{1 + \alpha} \right)^{4/3},$$

(9)

where A_0 is the contact area at zero applied load, and F_C is the minimum, or "critical," applied

load, corresponding to an instability in the tensile regime of the area-load curve ($F_C < 0$). While

F_C is typically equal to the pull-off force in an experiment, pull-off can also occur prematurely, or "early," (*i.e.*, for $F_N > F_C$), in which case the magnitude of the measured pull-off force is less than the true adhesive force, $|F_C|$. The dimensionless fitting parameter, α, identifies the mechanical nature of the contact, and its physical origin can be traced back to Tabor's parameter. In fact, both A_0 and F_C depend on α, as they are directly related to the deformability of the contact and the range of interaction. In addition to identifying the location of the contact along the JKR-DMT spectrum, the value of α can be used to determine whether the use of continuum mechanics models is appropriate for the nanoscale interface, or, conversely, whether the continuum approach breaks down at this scale. α is connected to μ_T via Maugis' parameter, λ, a simplified version of μ_T obtained using a square-well potential. In the COS equations, α is related to λ numerically, and this leads to the following approximation for the experimentally-determined μ_T:

$$\mu_T(\alpha) \approx -0.7986 \ln(1 - 1.02\alpha). \qquad (10)$$

If this experimental value is significantly different from a separate estimation of μ_T that is based on physically reasonable values for z_0 and K (as described in detail elsewhere [Grierson, 2005]), then it is possible that this continuum approach is inappropriate for the interface, or that the assumption of a constant shear strength is false. If w is known separately, comparison of Eqs. (8) and (10) can be performed without calibrating the normal and lateral forces, as α does not depend on C_N or C_L.

Once the calibration and fitting procedures are complete, w and τ_0 are calculated from α, R and K, according to the following relations:

$$w = \frac{-F_C}{\hat{F}_C(\alpha)\pi R}. \tag{11}$$

$$\tau_0 = \frac{F_{f,0}}{A_0}, \tag{12}$$

where

$$A_0 = \left(\frac{\pi w R^2}{K}\right)^{2/3} \hat{A}_0(\alpha). \tag{13}$$

The dimensionless, α-dependent terms, $\hat{A}_0$ and $\hat{F}_C$, emerge from the fit, as outlined in the original COS paper [Carpick, 1997b]. In this procedure, it is typical to use bulk values for the elastic constants. While this approach has produced reasonable results in certain cases, it is important to consider that it may fail in others. Moreover, while a sphere-on-flat is often a good approximation for the interfacial geometry, tip shape has a strong impact on the area-load relation [Carpick, 1996]. In addition to the use of electron microscopy to characterize tip shape [Kopycinska-Müller, 2006], the blind reconstruction scheme of Villarubia allows tip shape to be extracted from topographic images of sharp nanoscale features [Villarrubia, 1996; Villarrubia, 1997; Dongmo, 2000]. If early pull-off occurs, it may be necessary to consider in the analysis the effect of contact area reduction, or "microslip," caused by the applied shear stress [Johnson, 1997; Unertl, 1999].

Up until this point, it has been assumed that the shear strength is independent of load. This assumption precludes an unbiased understanding of the intrinsic frictional response at an interface. As discussed above, if a continuum fit is applied directly to friction-load

measurements, a discrepancy between calculated and estimated Tabor's parameters may indicate that this assumption is incorrect (though it may also indicate that continuum methods are altogether inapplicable). There are at least two ways to measure contact area directly and thereby resolve this dilemma: (1) lateral stiffness and (2) electrical conductance measurements. Conductance increases with contact area and thus varies with load [Pethica, 1979], permitting the independent measurement of area-load relationships in an AFM. This has been demonstrated for a tungsten carbide tip on boron-doped diamond [Enachescu, 1998]. However, the requirement that both materials be conducting restricts the use of contact conductance measurements to a small subset of friction-load experiments. On the other hand, lateral stiffness measurements are, in principle, useful for any interface. The measurement is accomplished by a lock-in technique described elsewhere [Carpick, 1997c; Lantz, 1997a].

In an AFM, the total lateral stiffness is given by the torsional spring constant of the cantilever, the lateral stiffness (bending) of the tip shaft, and the lateral contact stiffness:

$$k_{L,total}^{-1} = k_{L,cantilever}^{-1} + k_{L,tip}^{-1} + k_{L,contact}^{-1} . \tag{14}$$

The contribution from $k_{L,tip}$ is important to consider for tip shafts with high aspect ratios. Furthermore, it has been shown that the low contact area of sharp tips can lead to contact stiffnesses comparable to the torsional spring constant of the cantilever, and thus have a significant impact on the calculation of lateral forces [Lantz, 1997a; Piétrement, 1999]. The lateral contact stiffness arises from the gradient of the interaction force between atoms on the tip and sample. These individual springs act in parallel. As a result, their contributions are summed together, and their total effect is proportional to the contact area. Hence, the contact stiffness is

generally a function of the applied load. Lateral stiffness measurements yield $k_{L,total}$; therefore, $k_{L,cantilever}$ and $k_{L,tip}$ must be determined separately in order to extract $k_{L,contact}$. Furthermore, for a sphere-on-flat geometry, the equation relating lateral contact stiffness to contact area,

$$k_{L,contact} = 8G^* \sqrt{\frac{A}{\pi}}, \tag{15}$$

depends on prior knowledge of the combined shear modulus, $G^* = \left(\dfrac{2 - v_{tip}}{G_{tip}} + \dfrac{2 - v_{sample}}{G_{sample}} \right)^{-1}$,

where G is the shear modulus of the tip or sample. For their measurements, Lantz *et al*. used bulk values for G^* and demonstrated good agreement in comparison with continuum theory [Lantz, 1997b]. If the relevant elastic moduli are known, lateral stiffness *vs*. load measurements yield the area-load relation:

$$A(F_N) = \frac{\pi k_{L,contact}^2 (F_N)}{64 G^{*2}}. \tag{16}$$

$\tau(F_N)$ is obtained by combining Eqs. (6) and (16). In this way, any pressure (or load) dependence of the shear strength is revealed. Otherwise, dividing the two experimentally-obtained quantities, F_L and $k_{L,contact}^2$, yields the simple proportionality:

$$\frac{F_L}{k_{L,contact}^2} = \frac{\pi \tau_0}{64 G^{*2}}. \tag{17}$$

Multiple authors have determined lateral stiffness and contact area as a function of applied load for various materials and conditions, using this technique [Carpick, 1997c; Lantz, 1997a;

Lantz, 1997b; Piétrement, 2001a & 2001b; Wahl, 1998]. Piétrement *et al*. further developed the lateral stiffness measurement technique to avoid the use of elastic constants in the contact area calculation completely [Piétrement, 2001b]. Alternatively, contact stiffness measurements may be used to calculate local elastic properties [Reinstädtler, 2005; Hurley, 2007 & 2010]. Altogether, lateral stiffness measurements have provided independent confirmation of Bowden and Tabor's hypothesis that friction is proportional to contact area.

III. Outlook for nanoscale devices

It is critical to emphasize that the analysis presented in Section II is based on the assumption that continuum methods accurately model nanoscale contacts. Simulations of atomistic behavior have shown that deviations from a continuum approach can occur, depending on the atomic-level geometry of the contact. In addition to the general shape (*e.g*., parabolic, flat punch, *etc*.) or the nanoscale roughness of the contacting bodies, the relative arrangement of atoms at the interface can have a strong impact on nanoscale friction and area-load relations. This is underscored by the existence of atomic-level stick-slip. The following atomic-scale geometries have been simulated: commensurate (where the two surfaces have coincident or perfectly matched periodicities or some degree of overlap), incommensurate (where they exhibit no overlap), or amorphous (where at least one surface consists of randomly arranged atoms). In their simulations, Müser *et al*. found that rigid, incommensurate surfaces can interlock with each other only in the presence of mobile atoms or a diffusing film (or fluid) at their interface [Müser, 2000 & 2001]. This leads to increased static friction. If the two materials are incommensurate, but at least one of them is

sufficiently compliant, local stresses can cause the atoms at their interface to move into interlocking positions. Surprisingly, the same study by Müser *et al*. found that, although the diffusing atoms in the film are mobile, they fail to dislodge a commensurate interface. In fact, based on their findings, a thin fluid layer can cause interlocking between commensurate and incommensurate surfaces, alike. Separately, Kim and Hurtado have studied length scale effects: Based on a dislocation-assisted slip model, they predict that the shear strength should increase as the tip radius (or object size) decreases [Kim, 2000b; Hurtado 1999a & 1999b]. The implications for M/NEMS devices are profound.

Returning to issues of M/NEMS reliability, it should be noted that friction and wear are inextricably related. High shear stress caused by large lateral forces (friction) leads to wear. If the interaction between atoms at an interface is relatively low and the corrugated surface potential shallow, then sliding can be easy for atomically smooth surfaces, and the bonds between the atoms and their substrates are less likely to stretch and break. Observations of macroscale phenomena support this interpretation; however, aside from very recent work [Gotsmann, 2008; Lantz, 2009; Bhaskaran, 2010], few studies have focused directly on the impact of shear stress on wear at the *atomic* level. As with friction, it is clear from these studies that macroscopic models do not accurately represent nanoscale observations, but a full understanding of atomic-scale wear has not yet emerged. The combination of electron microscopy and AFM or similar tools to observe mechanical deformation (both elastic and plastic) and materials transformations is an enabling technology in this respect [Erts, 2002; Cumings, 2000]. In particular, the TEM has enabled the *in situ* observation of atomic-level phenomena, including, for example, the mechanical annealing of defects in nanoscale structures

[Shan, 2008] and the formation of single-atom-thick gold wires [Takai, 2001]. Further use of combined AFM/TEM instruments for tribological measurements would enhance the understanding of both frictional energy dissipation and atomic-scale wear.

While it is important to understand the impact of different parameters and conditions to improve tribological behavior, it is also interesting to approach new discoveries as a means to harness the frictional properties of a material for high-precision manipulation and control. It is already known that nanoscale friction may be actively tuned (or switched off and on) either electronically [Park, 2006 & 2007] or by mechanical actuation [Socoliuc, 2006; Gnecco, 2009; Lantz, 2009]. Furthermore, atomic-level stick-slip can provide a ratcheting mechanism useful for high-precision positioning, with each step equal to an integer multiple of the spacing between surface atoms or lattice sites. In this respect, the scientific and technological knowledge gained from nanotribological measurements has the potential for advancements beyond improving the performance of M/NEMS devices.

References

Alexander, S., L. Hellemans, 0. Marti, J Schneir, V. Elings, P. K. Hansma, M. Longmire and J. Gurley, 1989, "An atomic-resolution atomic-force microscope implemented using an optical lever," J. Appl. Phys., **65**, pp. 164-167.

Asay, D. B., M. T. Dugger, J. A. Ohlhausen and S. H. Kim, 2008a, "Macro- to nanoscale wear prevention via molecular adsorption," Langmuir, **24**, pp. 155-159.

Asay, D. B., M. T. Dugger and S. H. Kim, 2008b, "In-situ vapor-phase lubrication of MEMS," Tribol. Lett., **29**, pp. 67-74.

Bhaskaran, H., B. Gotsmann, A. Sebastian, U. Drechsler, M. A. Lantz, M. Despont, P. Jaroenapibal, R. W. Carpick, Y. Chen and K. Sridharan, 2010, "Ultralow nanoscale wear through atom-by-atom attrition in silicon-containing diamond-like carbon," Nature Nanotechnol., **5**, pp. 181-185.

Binnig, G. and H. Rohrer, 1982, "Scanning tunneling microscope," U. S. Patent, 4,343,993 (3 pages).

Binnig, G. and H. Rohrer, 1983, "Surface imaging by scanning tunneling microscopy," Ultramicroscopy, **11**, pp. 157-160.

Binnig, G., C. F. Quate and C. Gerber, 1986, "Atomic force microscope," Phys. Rev. Lett., **56**, pp. 930-933.

Bowden, F. P. and D. Tabor, 1985, *The Friction and Lubrication of Solids*, Clarendon Press: Oxford, England.

Briscoe, B. J. and D. C. B. Evans, 1982, "The shear properties of Langmuir-Blodgett layers," Proc. R. Soc. Lond. A, **380**, pp. 389-407.

Burnham, N. A., X. Chen, C. S. Hodges, G. A. Matei, E. J. Thoreson, C. J. Roberts, M. C. Davies and S. J. B. Tendler, 2003, "Comparison of calibration methods for atomic force microscopy cantilevers," Nanotechnology, **14**, pp. 1-6.

Burns, A. R., J. E. Houston, R. W. Carpick and T. A. Michalske, 1999, "Friction and molecular deformation in the tensile regime," Phys. Rev. Lett., **82**, pp. 1181-1184.

Butt, H.-J. and M. Jaschke, 1995, "Calculation of thermal noise in atomic force microscopy," Nanotechnology, **6**, pp. 1–7.

Cain, R. G., M. G. Reitsma, S. Biggs and N. W. Page, 2001, "Quantitative comparison of three calibration techniques for the lateral force microscope," Rev. Sci. Instrum., **72**, pp. 3304-3312.

Cannara, R. J., M. J. Brukman and R. W. Carpick, 2005, "Cantilever tilt compensation for variable-load atomic force microscopy," Rev. Sci. Instrum., **76**, 053706 (6 pp).

Cannara, R. J., M. Eglin and R. W. Carpick, 2006, "Lateral force calibration in atomic force microscopy: A new lateral force calibration method and general guidelines for optimization," Rev. Sci. Instrum., **77**, 053701 (11 pp).

Carpick, R. W., N. Agraït, D. F. Ogletree and M. Salmeron, 1996, "Measurement of interfacial shear (friction) with an ultrahigh vacuum atomic force microscope," J. Vac. Sci. Technol. B, **14**, pp. 1289-1295.

Carpick, R. W. and M. Salmeron, 1997a, "Scratching the surface: Fundamental investigations of tribology with atomic force microscopy," Chem. Rev., **97**, pp. 1163-94.

Carpick, R. W., D. F. Ogletree and M. Salmeron, 1997b, "A general equation for fitting contact area and friction *vs*. load measurements," J. Coll. Interf. Sci., **211**, pp. 395-400.

Carpick, R. W., D. F. Ogletree and M. Salmeron, 1997c, "Lateral stiffness: A new nanomechanical measurement for the determination of shear strengths with friction force microscopy," Appl. Phys. Lett., **70**, pp. 1548-1550.

Chung, K.-H. and M. G. Reitsma, 2007, "Note: Lateral force microscope calibration using multiple location pivot loading of rectangular cantilevers," Rev. Sci. Instrum., **81**, 026104 (3 pp).

Chung, K.-H., J. R. Pratt and M. G. Reitsma, 2010, "Lateral force calibration: Accurate procedures for colloidal probe friction measurements in atomic force microscopy," Langmuir, **26**, pp. 1386-1394.

Cleveland, J. P., S. Manne, D. Bocek and P. K. Hansma, 1993, "A nondestructive method for determining the spring constant of cantilevers for scanning probe microscopy," Rev. Sci. Instrum., **64**, pp. 403–405.

Colton, R. J., 2004, "Nanoscale measurements and manipulation," J. Vac. Sci. Technol. B, **22**, pp. 1609-1635.

Cumings, J. and A. Zettl, 2000, "Low-friction nanoscale linear bearing realized from multiwall carbon nanotubes," Science, **289**, pp. 602-604.

Derjaguin, B. V., V. M. Muller and Y. P. Toporov, 1975, "Effect of contact deformations and the adhesion of particles," J. Colloid Interf. Sci., **53**, pp. 314–326.

Derose, J. A. and J.-P. Revel, 1997, "Examination of atomic (scanning) force microscopy probe tips with the electron microscope," Microsc. Microanal., **3**, pp. 203-213.

Dongmo, L. S., J. S. Villarrubia, S. N. Jones, T. B. Renegar, M. T. Postek and J. F. Song, 2000, "Experimental test of blind tip reconstruction for scanning probe microscopy," Ultramicroscopy, **85**, pp. 141-153.

Edwards, S. A., W. A. Ducker and J. E. Sader, 2008, "Influence of atomic force microscope cantilever tilt and induced torque on force measurements," J. Appl. Phys., **103**, 064513 (6 pp).

Erts, D., A. Lõhmus, R. Lõhmus, H. Olin, A. V. Pokropivny, L. Ryen and K. Svensson, 2002, "Force interactions and adhesion of gold contacts using a combined atomic force microscope and transmission electron microscope," Appl. Surf. Sci., **188**, pp. 460-466.

Enachescu, M., R. J. A. van den Oetelaar, R. W. Carpick, D. F. Ogletree, C. F. J. Flipse and M. Salmeron, 1998, "Atomic force microscopy study of an ideally hard contact: The diamond(111)/tungsten carbide interface," Phys. Rev. Lett., **81**, pp. 1877-1880.

Feiler, A., P. Attard and I. Larson, 2000, "Calibration of the torsional spring constant and the lateral photodiode response of frictional force microscopes," Rev. Sci. Instrum., **71**, pp. 2746-2750.

Fushinobu, K., L. M. Phinney and N. C. Tien, 1996, ''Ultrashort-pulse laser heating of silicon to reduce microstructure adhesion,'' Int. J. Heat & Mass Transfer, **39**, pp. 3181–3186.

Gates, R. S. and M. G. Reitsma, 2007, "Precise atomic force microscope spring constant calibration using a reference cantilever array," Rev. Sci. Instrum., 78, 086101 (3 pp).

Gibson, C. T., G. S. Watson and S. Myhra, 1996, "Determination of the spring constants of probes for force microscopy/spectroscopy," Nanotechnology, **7**, pp. 259-262.

Gnecco, E., R. Bennewitz, T. Gyalog and E. Meyer, 2001, "Friction experiments on the nanometre scale," J. Phys.: Condens. Matter, **13**, pp. R619-R642.

Gnecco, E., A. Socoliuc, S. Maier, J. Gessler, T. Glatzel, A. Baratoff and E. Meyer, 2009, "Dynamic superlubricity on insulating and conductive surfaces in ultra-high vacuum and ambient environment," Nanotechnology, **20**, 025501 (7 pp).

Gotsmann, B. and M. A. Lantz, 2008, "Atomistic wear in a single asperity sliding contact," Phys. Rev. Lett., **101**, 125501 (4 pp).

Green, C. P., H. Lioe, J. P. Cleveland, R. Proksch, P. Mulvaney and J. E. Sader, 2004, "Normal and torsional spring constants of atomic force microscope cantilevers," Rev. Sci. Instrum., **75**, pp. 1988-1996.

Greenwood, J. A. and J. B. P. Williamson, 1966, "Contact of nominally flat surfaces," Proc. Roy. Soc. Lond. A, **295**, pp. 300-319.

Greenwood, J. A., 1997, "Adhesion by elastic spheres," Proc. R. Soc. Lond. A, **453**, pp. 1277–1297.

Grierson, D. S., E. E. Flater and R. W. Carpick, 2005, "Accounting for the JKR-DMT transition in adhesion and friction measurements with atomic force microscopy," J. Adhesion Sci. Technol., **19**, pp. 291-311.

Guckel, H., J. J. Sniegowski, T. R. Christenson and F. Raissi, 1990, "The application of fine-grained, tensile polysilicon to mechanicaly resonant transducers," Sens. Actuators A, **21**, pp. 346-351.

Hähner, G. and N. Spencer, 1998, "Rubbing and scrubbing," Phys. Today, **51**, pp. 22-27.

Henck, S. A., 1997, "Lubrication of digital micromirror devices TM," Tribol. Lett., **3**, pp. 239-247.

Houston, J. E. and T. A. Michalske, 1992, "The interfacial-force microscope," Nature, **356**, pp. 266-267.

Houston, J. E. and H. I. Kim, 2002, "Adhesion, friction, and mechanical properties of functionalized alkanethiol self-assembled monolayers," Acc. Chem. Res., **35**, pp. 547-553.

Hurley, D. C. and J. A. Turner, 2007, "Measurement of Poisson's ratio with contact-resonance atomic force microscopy," J. Appl. Phys., **102**, 033509 (8 pp).

Hurley, D. C., 2010, "Measuring mechanical properties on the nanoscale with contact resonance force microscopy methods," in *Scanning Probe Microscopy of Functional Materials: Nanoscale Imaging and Spectroscopy*, S. Kalinin and A. Gruverman (Eds.), Springer-Verlag: Berlin, Germany, in press.

Hurtado, J. A. and K.-S. Kim, 1999a, "Scale effects in friction of single-asperity contacts. I. From concurrent slip to single-dislocation-assisted slip," Proc. R. Soc. Lond. A, **455**, pp. 3363-3384.

Hurtado, J. A. and K.-S. Kim, 1999b, "Scale effects in friction of single-asperity contacts. II. Multiple-dislocation-cooperated slip," Proc. R. Soc. Lond. A, **455**, pp. 3385-3400.

Hutchings, I. M., 1992, *Tribology—Friction and Wear of Engineering Materials*, CRC Press: Boca Raton, FL.

Hutter, J. L. and J. Bechhoefer, 1993, "Calibration of atomic force microscope tips," Rev. Sci. Instrum., **64**, pp. 1868–1873.

Johnson, K. L., K. Kendall and A. D. Roberts, 1971, "Surface energy and the contact of elastic solids," Proc. R. Soc. Lond. A, **324**, pp. 301–313.

Johnson, K. L., 1997, "Adhesion and Friction between a Smooth Elastic Spherical Asperity and a Plane Surface," Proc. R. Soc. Lond. A, **453**, pp. 163-179.

Jost, P., 1966, "Lubrication (Tribology)—A Report on the Present Position and Industry's Needs," Department of Education and Science, H.M. Stationary Office, London.

Jost, P., 1976, "Economic impact of tribology," Proc. Mechanical Failures Prevention Group, NBS Special Pub., **423**, Gaithersburg, MD.

Joyce, S. A. and J. E. Houston, 1991, "A new force sensor incorporating force-feedback control for interfacial force microscopy," Rev. Sci. Instrum., **62**, pp. 710-715.

Kiely, J. D. and J. E. Houston, 1999, "Contact hysteresis and friction of alkanethiol self-assembled monolayers on gold," Langmuir**, 15**, pp. 4513-4519.

Kim, H. I. and J. E. Houston, 2000a, "Separating mechanical and chemical contributions to molecular-level friction," J. Am. Chem. Soc., **122**, pp. 12045-12046.

Kim, K.-S. and J. A. Hurtado, 2000b, "Length-scale effects in nano- and micro-mechanics of solids," Fracture and Strength of Solids, Key Engineering Materials, **183-1**, pp. 1-7.

Kim, S. H., D. B. Asay and M. T. Dugger, 2007, "Nanotribology and MEMS," NanoToday, **2**, pp. 22-29.

Kopycinska-Müller, M., R, H. Geiss and D. C. Hurley, 2006, "Contact mechanics and tip shape in AFM-based nanomechanical measurements," Ultramicroscopy, **106**, pp. 466-474.

Lantz, M. A., S. J. O'shea, A. C. F. Hoole and M. E. Welland, 1997a, "Lateral stiffness of the tip and tip-sample contact in frictional force microscopy," Appl. Phys. Lett., **70**, pp. 970-972.

Lantz, M. A., S. J. O'shea, M. E. Welland and K. L. Johnson, 1997b, "Atomic-force-microscope study of contact area and friction on $NbSe_2$," Phys. Rev. B, **55**, pp. 10776-10784.

Lantz, M. A., D. Wiesmann and B. Gotsmann, 2009, "Dynamic superlubricity and the elimination of wear on the nanoscale," Nature Nanotech., **4**, pp. 586-589.

Li, Q., K.-S. Kim and A. Rydberg, 2006, "Lateral force calibration of an atomic force microscope with a diamagnetic levitation spring system," Rev. Sci. Instrum., **77**, 065105 (13 pp). (See also the online resource http://www.engin.brown.edu/facilities/nanomicro/calibrator/dlfcindex.html for instructions on implementing the technique.)

Lin, S.C. and K. Banerjee, 2008, "Cool chips: opportunities and implications for power and thermal management," IEEE Trans. Electron Devices, **55**, pp. 245-255.

Luan, B. and M. O. Robbins, 2005, "The breakdown of continuum models for mechanical contacts," Nature, **435**, pp. 929-932.

Luan, B. and M. O. Robbins, 2006, "Contact of single asperities with varying adhesion: Comparing continuum mechanics to atomistic simulations," Phys. Rev. E, **74**, 026111 (17 pp).

Luo, J. K., Y. Q. Fu, H. R. Le, J. A. Williams, S. M. Spearing and W. I. Milne, 2007, "Diamond and diamond-like carbon MEMS," J. Micromech. Microeng., **17**, pp. S147–S163.

Maboudian, R. and R. T. Howe, 1997, ''Critical review: adhesion in surface micromechanical structures,'' J. Vac. Sci. Technol. B, **15**, pp. 1–20.

Maboudian R. and C. Carraro, 2003, "Surface engineering for reliable operation of MEMS devices," J. Adh. Sci. Technol., **17**, pp. 583-591.

Major, R. C., H. I. Kim, J. E. Houston and X.-Y. Zhu, 2003, "Tribological properties of alkoxyl monolayers on oxide terminated silicon," Tribol. Lett., **14**, pp. 237-244.

Major, R. C., J. E. Houston, M. J. McGrath, J. I. Siepmann and X.-Y. Zhu, 2006, "Viscous water meniscus under nanoconfinement," Phys. Rev. Lett., **96**, 177803 (4 pp).

Marti, O., J. Colchero and J. Mlynek, 1990, "Combined scanning force and friction microscopy of mica," Nanotechnology, **1**, pp. 141-144.

Mate, C. M., G. M. McClelland, R. Erlandsson and S. Chiang, 1987, "Atomic-scale friction of a tungsten tip on a graphite surface," Phys. Rev. Lett., **59**, pp. 1942-1945.

Maugis, D., 1992, "Adhesion of spheres: The JKR-DMT transition using a Dugdale model," J. Colloid Interface Sci., **150**, pp. 243-269.

Meyer, E., R. Overney, K. Dransfeld and T. Gyalog, 1998, *Nanoscience: Friction and Rheology on the Nanometer Scale*, Singapore: World Scientific.

Meyer, G. and N. M. Amer, 1988, "Novel optical approach to atomic force microscopy," Appl. Phys. Lett., **53**, pp. 1045-1047.

Meyer, G. and N. M. Amer, 1990a, "Optical-beam-deflection atomic force microscopy: The NaCl (001) surface," Appl. Phys. Lett., **56**, pp. 2100-2101.

Meyer, G. and N. M. Amer, 1990b, "Simultaneous measurement of normal and lateral forces with an optical-beam-deflection atomic force microscope," Appl. Phys. Lett., **57**, pp. 2089-2091.

Mo, Y., K. T. Turner and I. Szlufarska, 2009, "Friction laws at the nanoscale," Nature, **457**, pp. 1116-1119.

Morita, S., S. Fujisawa and Y. Sugawara, 1996, "Spatially quantized friction with lattice periodicity," Surface Science Reports, **23**, pp. 1-41.

Mulhern, G. T., D. S. Soane and R. T. Howe, 1993, "Supercritical carbon dioxide drying of microstructures," Proc. 7th Int. Conf. Solid-State Sensors and Actuators (Transducers), Yokohama, Japan, pp. 296-300.

Munz, M., 2010, "Force calibration in lateral force microscopy: a review of the experimental methods," J. Phys. D: Appl. Phys., **43**, 063001 (34 pp).

Müser, M. H. and M. O. Robbins, 2000, "Conditions for static friction between flat crystalline surfaces," Phys. Rev. B, **61**, pp. 2335-2342.

Müser, M. H., L. Wenning and M. O. Robbins, 2001, "Simple microscopic theory of Amontons's laws for static friction," Phys. Rev. Lett., **86**, pp. 1295-1298.

Obraztsov, A. N., P. G. Kopylov, B. A. Logynov, M. A. Dolganov, R. R. Ismagilov and N. V. Savenko, 2010, "Single crystal diamond tips for scanning probe microscopy," Rev. Sci. Instrum., **81**, 013703 (4 pp).

Ogletree, D. F., R. W. Carpick and M. Salmeron, 1996, "Calibration of frictional forces in atomic force microscopy," Rev. Sci. Instrum., **67**, pp. 3298-3306.

Olivero, P., S. Rubanov, P. Reichart, B. C. Gibson, S. T. Huntington, J. R. Rabeau, A. D. Greentree, J. Salzman, D. Moore, D. N. Jamieson and S. Prawer, 2006, "Characterization of three-dimensional microstructures in single-crystal diamond," Diamond Rel. Mater., **15**, pp. 1614-1621.

Park, J. Y, D. F. Ogletree, P. A. Thiel and M. Salmeron, 2006, "Electronic control of friction in silicon pn junctions," Science, **313**, p. 186.

Park, J. Y., Y. Qi, D. F. Ogletree, P. A. Thiel and M. Salmeron, 2007, "Influence of carrier density on the friction properties of silicon *pn* junctions," Phys. Rev. B, **76**, 064108 (7 pp).

Peiner, E., A. Tibrewala, R. Bandorf, H. Lüthje, L. Doering and W. Limmer, 2007, "Diamond-like carbon for MEMS," J. Micromech. Microeng., **17,** pp. S83–S90.

Persson, B. N. J., 2000, *Sliding Friction: Physical Principles and Applications*, Springer-Verlag: Berlin, Heidelberg, Germany.

Pethica, J. B. and D. Tabor, 1979, "Contact of characterized metal surfaces at very low loads: Deformation and adhesion," Surf. Sci., **89**, pp. 182-190.

Phinney, L. M., K. Fushinobu and C. L. Tien, 2000, ''Subpicosecond laser processing of polycrystalline silicon microstructures,'' Microscale Thermophys. Eng., **4**, pp. 61–75.

Piétrement, O., J. L. Beaudoin and M. Troyon, 1999, "A new calibration method of the lateral contact stiffness and lateral force using modulated lateral force microscopy," Tribol. Lett., **7**, pp. 213-220.

Piétrement, O. and M. Troyon, 2001a, "Study of the interfacial shear strength pressure dependence by modulated lateral force microscopy," Langmuir, **17**, pp. 6540-6546.

Piétrement, O. and M. Troyon, 2001b, "Quantitative study of shear modulus and interfacial shear strength by combining modulated lateral force and magnetic force modulation microscopies," Surf. Interf. Anal., **31**, pp. 1060-1067.

Reitsma, M. G., 2007, "Lateral force microscope calibration using a modified atomic force microscope cantilever," Rev. Sci. Instrum., **78**, 106102 (3 pp).

Reinstädtler, M., T. Kasai, U. Rabe, B. Bhushan and W. Arnold, 2005, "Imaging and measurement of elasticity and friction using the TRmode," J. Phys. D: Appl. Phys., **38**, R269–R282.

Rogers, J. W. and L. M. Phinney, 2002, "Nanosecond laser repair of adhered MEMS structures," J. Heat Transfer, **124**, pp. 394-396.

Romig, Jr., A. D., M. Y. Dugger and P. J. McWhorter, 2003, "Materials issues in microelectromechanical devices: science, engineering, manufacturability and reliability," Acta Materialia, **51**, pp. 5837-5836.

Sader, J. E., 1999, "Calibration of rectangular atomic force microscope cantilevers," Rev. Sci. Instrum., **70**, pp. 3967-3969. (See also http://www.ampc.ms.unimelb.edu.au/afm/calibration.html for an online resource for calculating normal and lateral spring constants of rectangular cantilevers.)

Sader, J. E. and C. P. Green, 2004, "In-plane deformation of cantilever plates with applications to lateral force microscopy," Rev. Sci. Instrum., **75**, pp. 878-883.

Sader, J. E., J. Pacifico, C. P. Green and P. Mulvaney, 2005, "General scaling law for stiffness measurement of small bodies with applications to the atomic force microscope," J. Appl. Phys., **97**, 124903 (7 pp).

Schwarz, U. D., O. Zwörner, P. Köster and R. Wiesendanger, 1997, "Preparation of probe tips with well-defined spherical apexes for quantitative scanning force microscopy," J. Vac. Sci. Technol. B, **15**, pp. 1527-1530.

Schwarz, U. D., 2003, "A generalized analytical model for the elastic deformation of an adhesive contact between a sphere and a flat surface," J. Coll. Interf. Sci., **261**, pp. 99-106.

Sekaric, L., J. M. Parpia, H. G. Craighead, T. Feygelson, B. H. Houston and J. E. Butler, "Nanomechanical resonant structures in nanocrystalline diamond," Appl. Phys. Lett, **81**, pp. 4455-4457.

Shan, Z. W., R. K. Mishra, S. A. S. Asif, O. L. Warren and A. M. Minor, 2008, "Mechanical annealing and source-limited deformation in submicrometre-diameter Ni crystals," Nature, **7**, pp. 115-119.

Socoliuc, A., E. Gnecco, S. Maier, O. Pfeiffer, A. Baratoff, R. Bennewitz and E. Meyer, 2006, "Atomic-scale control of friction by actuation of nanometer-sized contacts," Science, **313**, pp. 207-210.

Stachowiak, G. W. and A. W. Batchelor, 2005, *Engineering Tribology* (3rd Edition), Elsevier Butterworth-Heinemann: Boston, MA.

Stiernstedt, J., M. W. Rutland and P. Attard, 2005, "A novel technique for the in situ calibration and measurement of friction with the atomic force microscope," Rev. Sci. Instrum., **76**, 262508.

Sullivan, J. P., T. A. Friedmann and K. Hjort, 2001, "Diamond and amorphous carbon MEMS," MRS Bulletin, **26**, pp. 309-311.

Szlufarska, I., M. Chandross and R. W. Carpick, 2008, "Recent advances in single-asperity nanotribology," J. Phys. D: Appl. Phys., **41**, 123001 (39 pp).

Tabor, D., 1977, "Surface forces and surface interactions," J. Coll. Interf. Sci., **58**, pp. 2-13.

Takai, Y., T. Kawasaki, Y. Kimura, T. Ikuta and R. Shimizu, 2001, "Dynamic observation of an atom-sized gold wire by phase electron microscopy," Phys. Rev. Lett., **87**, 106105 (4 pp).

Tocha, E., H. Schönherr and G. J. Vancso, 2006, "Quantitative nanotribology by AFM: A novel universal calibration platform," Langmuir, **22**, pp. 2340-2350.

Tortonese, M. and M. Kirk, 1997, "Characterization of application specific probes for SPM," SPIE**, 3009**, pp. 53–60.

Unertl, W. N., 1999, "Implications of contact mechanics models for mechanical properties measurements using scanning force microscopy," J. Vac. Sci. Technol. A, **17**, pp. 1779-1786.

Varenberg, M., I. Etsion and G. Halperin, 2003, "An improved wedge calibration method for lateral force in atomic force microscopy," Rev. Sci. Instrum., **74**, pp. 3362-3367.

Villarrubia, J. S., 1996, "Scanned probe microscope tip characterization without calibrated tip characterizers," J. Vac. Sci. Technol. B, **14**, pp. 1518-1521.

Villarrubia, J. S., 1997, "Algorithms for scanned probe microscope image simulation, surface reconstruction**,** and tip estimation," J. Res. Natl. Inst. Stand. Technol., **102**, pp. 425-454.

Wahl, K. J., S. V. Stepnowski and W. N. Unertl, 1998, "Viscoelastic effects in nanometer-scale contacts under shear," Tribol. Lett., **5**, pp. 103-107.

Watson, G. S., B. P. Dinte, J. A. Blach-Watson and S. Myhra, 2004, "Friction measurements using force versus distance friction loops in force microscopy," Appl. Surf. Sci., **235**, pp. 38-42.

Williams, J. A., 1994, *Engineering Tribology*, Oxford University Press: Oxford, England.

Williams, J. A., 2006, "Tribology and MEMS," J. Phys. D: Appl. Phys., **39**, pp. R201–R214.